A Numerical Investigation of Effects of a Tilt of the Zero Wind Stress Curl Line on the Subduction Process

TOMOKO INUI* AND KIMIO HANAWA

Department of Geophysics, Graduate School of Science, Tohoku University, Aoba-ku, Sendai, Japan

(Manuscript received 27 June 1995, in final form 19 August 1996)

ABSTRACT

A three-dimensional ocean general circulation model is used to investigate the effects of an idealized, nonzonal wind stress curl on the subduction process in the subtropical gyre. Idealized zonal winds are used to force the model ocean. Analyses of potential vorticity, water particle trajectories, and tracer-injection experiments are conducted. Two characteristic features appear in response to the nonzonal distribution of the wind stress curl: an upwelling region occurs in the subtropical gyre, and a downwelling region extends northward in the northeastern corner of the subtropical gyre. In comparison to results obtained from a zonal wind stress curl, a pool region, where there is no signal from the surface of the subarctic region, shrinks, a ventilated region becomes deeper, and the subducted water has a wider range of potential density.

1. Introduction

The oceanic response to the wind forcing has been studied analytically by many authors, for instance, Stommel (1948) and Munk (1950). After these pioneering works, the general circulation has been studied by many researchers. These studies have examined the dependence of the general circulation on parameters such as the Ekman number and the Rossby number. However, the understanding of the horizontal structures has advanced more than the thermocline structure.

Welander (1971) used a continuously stratified model governed by a weakly dissipative nonlinear equation to show that isopycnals rise toward the equator according to the conservation of potential vorticity. His solutions, however, strongly depended on the boundary conditions, which were arbitrarily defined. Weakly dissipative nonlinear equations are mathematically difficult to understand and arbitrarities about boundary conditions were also make it difficult to obtain the exact solution of the thermocline structure.

Luyten et al. (1983, hereafter LPS) proposed the ‘‘ventilated thermocline’’ theory, which reproduced the vertical structure of the circulation clearly for the first time. Their model has a finite number of active layers with a prescribed surface density field in the steady nondissipative regime. South of the upper-layer outcrop line, the lower layers are shielded from direct wind forcing. Thus, the potential vorticity of the lower layer is conserved in this region. An analytical solution is obtained by LPS for cases where outcrop and wind stress curl lines are oriented zonally. The solution has critical trajectories that separate the ventilated region, generated by Ekman pumping, from the eastern unventilated region, called the shadow zone, and the western unventilated regions, called the pool region. In order to consider various effects that a simple layer model does not include, numerical models are required. Cox and Bryan (1984, hereafter CB) studied the subduction process with a zonally uniform wind stress curl using a general circulation model. They examined the balance of each term in the density equation to find that the overturning term is the most important for the subduction process and that the ventilated region is fed by water cooled in the western boundary outflow region. They also showed a map of the advective subduction age on an isopycnal: This is the time taken for water particles to move from the sea surface to the last point of the subduction. They determined that it takes 10–15 years for water particles to circulate through the ventilated region in their model. There are many other studies of the subduction process that use a modified version of the LPS model, all with a zonally uniform wind stress curl. Various studies have attempted to include thermal effects: Pedlosky et al. (1984) added a mixed layer, and Pedlosky (1986) allowed exchange between layers. There are also studies using the continuously stratified model of Huang (1988), which also intend to include the thermal effects by considering a mixed layer (e.g., Pedlosky and Robbin 1991; Williams 1991).

* Current affiliation: Institute of Low Temperature Science, Hokkaido University, Sapporo, Japan.

Corresponding author address: Dr. Tomoko Inui, Institute of Low Temperature Science, Hokkaido University, Sapporo 060, Japan.
E-mail: inui@clim.lowtem.hokudai.ac.jp

© 1997 American Meteorological Society

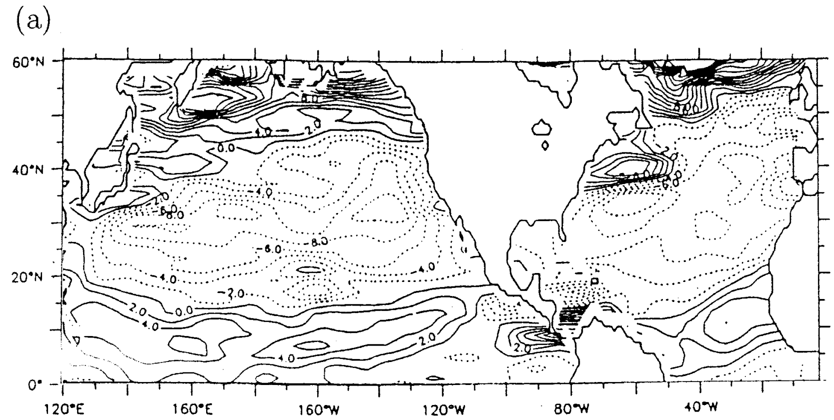

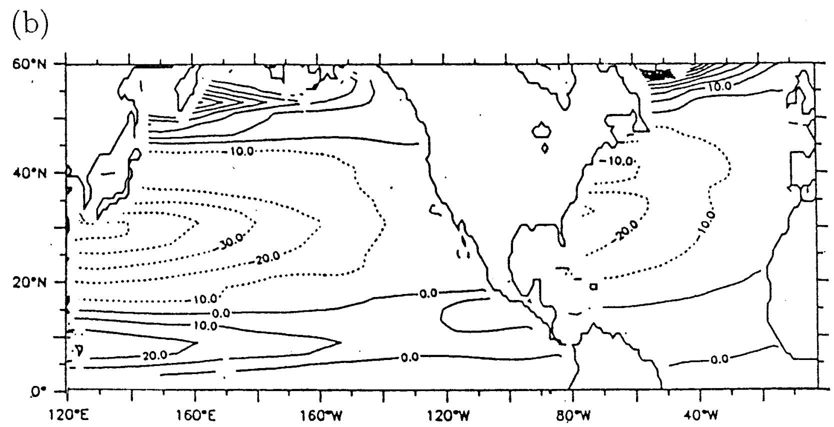

FIG. 1. Annual average wind stress curl (a) and annual average Sverdrup transport (b) in the North Pacific and Atlantic after Harrison (1988). Contour interval is 2×10^{-9} dyn cm^{-3} for (a) and 10^6 m^3 s^{-1} for (b). Solid and dashed curves indicate positive and negative values, respectively.

However, even with the studies mentioned above, it is still difficult to explain the observed distributions of tracers—the subduction process is highly complicated. Subduction could be estimated if it were possible to measure an Ekman pumping velocity directly. Since this is not possible, we have to examine the distribution of various tracers or water properties, for example, the shallow salinity minimum (SSM) water (e.g., Reid 1973; Tsuchiya 1982; Yuan and Talley 1992), in order to visualize the subduction process in the real ocean. In general, the source region of a tracer is considered to be an outcrop line within a downwelling region. This combination, outcrop line in downwelling region, is determined by the distribution of the wind stress curl. Most of the studies mentioned above, including LPS and CB, however, used a zonally uniform wind stress curl in their studies. Harrison (1988) (Fig. 1a) shows that the actual distribution of the wind stress curl is nonzonal in the climatological mean field. In fact, if we consider Fig. 1b, we see that the line defined by $\psi = 0$ (ψ: Sverdrup streamfunction) and the zero wind stress curl line actually lie at angles to each other. Next, we refer to some other studies that consider winds with a nonzonal zero wind stress curl line.

Talley (1985), using the LPS model with three active layers, studied an idealized subtropical gyre in a rectangular basin driven by an Ekman pumping velocity field. This field had a nonzonal boundary between regions of positive and negative vertical velocities. She showed that some streamlines that, originating at the western boundary south of the outcrop, surfaced into an outcrop region and then subducted. She also applied observed annual-average fields of wind stress, surface density, and surface salinity to an idealized basin and predicted the distribution of the SSM in the North Pacific. Huang (1989) used a continuously stratified model to calculate the wind-driven circulation using realistic North Atlantic surface boundary conditions, including a nonzonal zero wind stress curl line. He also considered a formulation that had a finite mixed layer whose depth was allowed to vary horizontally and with a nonzero density gradient. With this new formulation mentioned above, he concluded that the formation of a low potential vorticity water mass was increased and the circulation in the ventilated thermocline was intensified. Although his study uses actual, and therefore nonzonal, wind stress curl fields, which form an angle with the $\psi = 0$ line, he did not intend to isolate the effects of nonzonality. Rhines and Schopp (1991) used an eddy-resolving, three-layer, quasigeostrophic model to study general circulation forced by wind curl fields whose zero wind stress curl line (ZWCL) was not zonal. Their study implies that a region corresponding to the pool region in LPS becomes smaller and a region corresponding to the ventilated region in LPS becomes larger as the inclination of the ZWCL increases. They suggested that the ventilated region becomes larger due to the extension of the Sverdrup interior.

Effects of the nonzonal ZWCL have also been investigated by analyzing observational data. Yuan and Talley (1992) suggested that the tilt of the ZWCL has effects on the formation and circulation of the middle salinity minimum (MSM) water. By analyzing the distribution of potential density, they found that the MSM originates from a narrow region in the northwestern part of the subtropical gyre. They indicated that the formation of the MSM occurs only when the outcrop and downwelling regions overlap.

Talley (1985) and Rhines and Schopp (1991) have studied the effects of the nonzonal ZWCL; however, their studies are not meant to investigate the detailed vertical structure of the circulation because of the limited vertical resolution in their models. In order to include the vertical structure, this study uses a general circulation model similar to the one used in CB to evaluate effects of the nonzonal ZWCL on the subduction process. Our model is forced by three different idealized wind stress fields and the results are compared with those of LPS. The remainder of this paper is organized as follows. In section 2, the model ocean is described. Results for the zonal ZWCL are presented in section 3. In section 4, the results for the zonal ZWCL and for the nonzonal ZWCL are compared in order to evaluate effects of the nonzonal ZWCL. In both sections 3 and 4, trajectories of water particles and the distribution of a passive tracer are analyzed. Finally, a summary and discussion are given in section 5.

2. Description of the model

The model used in this study is the primitive equation GFDL Modular Ocean Model (MOM ver. 1.1). Only the governing equations will be given here; for a more detailed description of the scheme see earlier works (e.g., Bryan 1969). The model basin is 40° wide, extends from the equator to 60°N, and is 3000 m deep. The horizontal resolution is 1° × 1°. The model ocean has 24 levels in the vertical, which are distributed in the water column as shown in Fig. 2b.

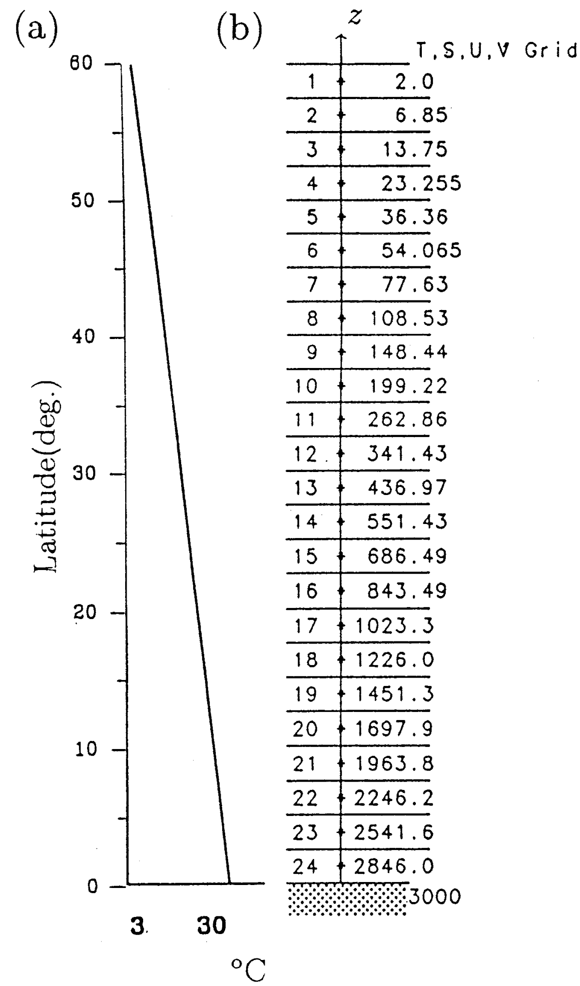

FIG. 2. (a) A meridional profile of the specified temperature T_a. (b) The arrangement of grid points in the vertical direction.

a. Governing equations

The equations of motion are the Navier–Stokes equations simplified by the Boussinesq and hydrostatic approximations. A spherical coordinate system is used, λ, ϕ, and z, representing longitude, latitude, and depth, respectively. The radius of the earth is represented by a. Salinity S is kept constant. The equations for horizontal velocity, (u, v), and potential temperature T are

$$u_t + \mathcal{L}(u) - \left(\frac{u\tan\phi}{a} + f\right)v = -\frac{1}{a\cos\phi}\left(\frac{P}{\rho_0}\right)_\lambda + F^u, \quad (1)$$

$$v_t + \mathcal{L}(v) + \left(\frac{u\tan\phi}{a} + f\right)u = -\frac{1}{a}\left(\frac{P}{\rho_0}\right)_\lambda + F^v, \quad (2)$$

$$T_t + \mathcal{L}(T) = F^T, \quad (3)$$

where the advection operator $\mathcal{L}$ is defined as

$$\mathcal{L}(\mu) = \frac{1}{a\cos\phi}[(u\mu)_\lambda + (v\mu\cos\phi)_\phi] + (w\mu)_z, \quad (4)$$

where μ represents either u, v, or T. The continuity equation is

$$\mathcal{L}(1) = 0. \tag{5}$$

The hydrostatic equation is

$$P_z = -\rho g. \tag{6}$$

The equation of state $\rho = \rho(T, S, z)$ is a third-order polynominal approximation to the UNESCO (1981) equation. In the above equations, $f = 2\Omega \sin\phi$ is the Coriolis parameter, P is the pressure, ρ is the density, and ρ_0 is set to be unity in cgs units.

The F terms represent the effects of turbulent viscosity and diffusion:

$$F^u = A_{\rm MV} u_{zz} + A_{\rm MH}\frac{1}{a^2} \times \left[\nabla^2 u + \left(1 - \frac{\sin^2\phi}{\cos^2\phi}\right)u - \frac{2\sin\phi}{\cos^2\phi}v_\lambda\right], \tag{7}$$

$$F^v = A_{\rm MV} v_{zz} + A_{\rm MH}\frac{1}{a^2} \times \left[\nabla^2 v + \left(1 - \frac{\sin^2\phi}{\cos^2\phi}\right)v - \frac{2\sin\phi}{\cos^2\phi}u_\lambda\right], \tag{8}$$

$$F^T = \left(\frac{A_{\rm TV}}{\delta}T_z\right)_z + \frac{A_{\rm TH}}{a^2}\nabla^2 T, \tag{9}$$

where

$$\delta = \begin{cases} 1, & \text{if } \rho_z \le 0 \\ 0, & \text{if } \rho_z > 0, \end{cases}$$

and the Laplacian operator is given by

$$\nabla^2\mu = \frac{1}{(\cos\phi)^2}\mu_{\lambda\lambda} + \frac{1}{\cos\phi}(\mu_\phi \cos\phi)_\phi. \tag{10}$$

The constants $A_{\rm MV}$ (vertical mixing coefficient for momentum), $A_{\rm MH}$ (horizontal mixing coefficient for momentum), $A_{\rm TV}$ (vertical mixing coefficient for tracer), and $A_{\rm TH}$ (horizontal mixing coefficient for tracer) are set to be 10, 10^8, 0.3, and 2×10^7 cm^2 s^{-1}, respectively. These coefficients are valid for all depths.

b. Boundary conditions

The model is forced by the zonal wind stress τ and by the surface heat flux Q. These are imposed at the ocean surface ($z = 0$) by the boundary conditions,

$$\rho_0 A_{\rm MV}(u_z, v_z) = (\tau, 0),\ w = 0,\ A_{\rm TV}T_z = Q. \tag{11}$$

The heat flux is assumed to have the Haney (1971) type flux form,

$$Q = \gamma(T_a - T_{\rm SST}), \tag{12}$$

where T_a represents a specified atmospheric temperature, $T_{\rm SST}$ is the model SST, and γ is set to be a constant 90 cm day^{-1}. The atmospheric temperature is a linear function of latitude only, 30°C at the equator and 5°C at 60°N (Fig. 2a).

The boundary conditions at the bottom ($z = -H$) are the zero-flux conditions

$$u_z = v_z = 0,\ w = 0,\ T_z = 0. \tag{13}$$

At all lateral walls, no-slip conditions are imposed and no flux of heat is allowed,

$$u = v = T_n = 0, \tag{14}$$

where the subscript n represents the local derivative normal to the wall.

c. Wind stress fields

We used the following zonal wind stress fields. When the ZWCL is zonal (RUN-1), τ is defined as

$$\tau = \begin{cases} 0.4\cos(2\pi\frac{y}{L}) - 0.6, & 0° < y < 20°\text{N} \\ \cos(2\pi\frac{y}{L}), & 20°\text{N} < y < 60°\text{N}. \end{cases} \tag{15}$$

Here L is 40° and y is latitudinal extent. When the ZWCL is not zonal (RUN-2 and RUN-3), it is defined following Rhines and Schopp (1991) as

$$\tau = \begin{cases} 0.4\cos(2\pi\frac{y}{L}) - 0.6, & 0° < y < 20°\text{N} \\ -\cos(2\pi\frac{\phi}{L}), & 20°\text{N} < y < 60°\text{N}, \end{cases} \tag{16}$$

where

$$\phi = y - Ax\sin\left(\frac{\pi y}{L}\right)$$

and x is longitudinal extent.

The value of $A = 0.1$ is used in RUN-2 to give a realistic distribution of the ZWCL, consistent with the annual mean distribution of the ZWCL in the North Pacific (Harrison 1988). The value of $A = 0.25$ is used in RUN-3 as an extreme case to emphasize the effects of the nonzonal ZWCL. The wind stress fields used for the three runs are illustrated in Fig. 3.

d. Initial conditions and integration

The model ocean is initially at rest and the temperature field is set to the zonally averaged climatological mean field (Levitus 1982). The salinity field is kept at a constant value of 34.9 psu everywhere, throughout the integration. After 40 years of integration at a one-hour time step, the model ocean, except in the abyssal part, reaches steady state for each of the three runs. We, therefore, used the results of the 40th year for our analyses of each run.

3. Solution for the zonal zero wind stress curl line

In this section, we will describe the results for the zonal ZWCL (RUN-1). Figure 4a shows the model SST

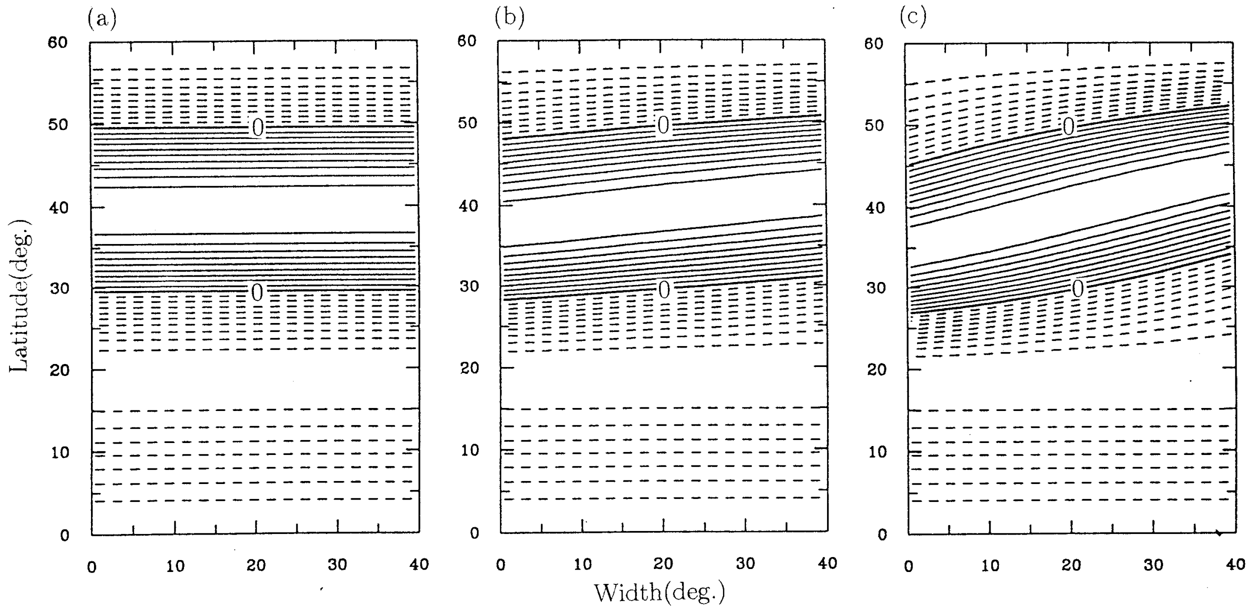

FIG. 3. Zonal wind stress fields used for (a) RUN-1, (b) RUN-2, and (c) RUN-3. Solid and dashed curves denote eastward and westward winds, respectively. The contour interval is 0.1 dyn cm^{-2}.

field, at the first level ($z = -2$ m). Isotherms are aligned mostly zonal, except in the midlatitude western boundary region where the warm water is advected into high latitude by the western boundary current. In the equatorial region, T has slightly lower values than those in the surrounding region. Figure 4b shows T at the 7th level ($z = -77.6$ m). This figure indicates that the thermocline tilts along the equator, which coincides with the core depth of the model undercurrent.

The simplified potential vorticity, $q = -f\rho_z$, is a useful tool to examine the subsurface circulation field. Figure 5a shows a meridional section of q in the middle of the basin. Low q water from the subarctic region is injected into the subtropical region, reaching a depth of approximately 200 m in the subtropical gyre. Maximum q water exists as the thermocline water below this low q water. Figure 5b shows the horizontal distribution of q on an isopycnal surface of potential density $\sigma_\theta = 26.1$. The depth of this isopycnal surface corresponds to that of the main thermocline in the subtropical gyre. This figure clearly indicates that low q water originating from the eastern outcrop region is subducted southwestward. Figure 5c shows q on the 8th level ($z = -108.5$ m). This depth corresponds roughly to the bottom of the mixed layer in the subtropical gyre. At this level, low q water penetrates southwestward from the subarctic region into the subtropical region. High q water extends northeastward from the separation point of the western boundary current. As this warm, high q water flows into higher latitudes, q decreases due to the negative heat flux. The overall tendency of the results is fairly similar to that of CB.

We analyzed the trajectories of water parcels to evaluate the timescale of the subduction process, as well as the origin and destination of the subducted water. We also performed a tracer injection experiment to visualize the subduction process. With this tracer it was possible to see water originating at the subarctic gyre move into the subtropical gyre due to diffusion and advection. The equation for tracer concentrations is given in the appendix. This calculation is started at the 40th year, and the variables u, v, and T are kept at the values found for the solution at year 40. Only the subarctic tracer is allowed to evolve over time. In this way, the tracer experiment determines the distribution of the tracer formed by a steady-state flow. Initially, the tracer has a value of zero everywhere. At year 40, the tracer concentration at the surface of the subarctic gyre is set and restored to a value of 100. This restoring is carried on throughout the 15 years of integration. As the integration proceeds, tracer concentrations increase in all regions.

According to the trajectory analysis (not shown here), the timescale of the subduction process is estimated to be 10 to 15 years. Figure 6 uses the distribution of subarctic tracer on an isopycnal surface of $\sigma_\theta = 26.1$ to indicate the temporal evolution of the subduction process. It shows clearly the three regions in the subtropical gyre discussed by LPS: 1) a pool region, located in the northwest of the subtropical region, where there is no signal of the subarctic tracer; 2) a ventilated region, located to the east of the pool region, effectively and smoothly fed by the subarctic tracer; and 3) a shadow zone, located to the south of the ventilated region, where there is no signal of the subarctic tracer. Based on the distribution of the tracer, the timescale of the subduction

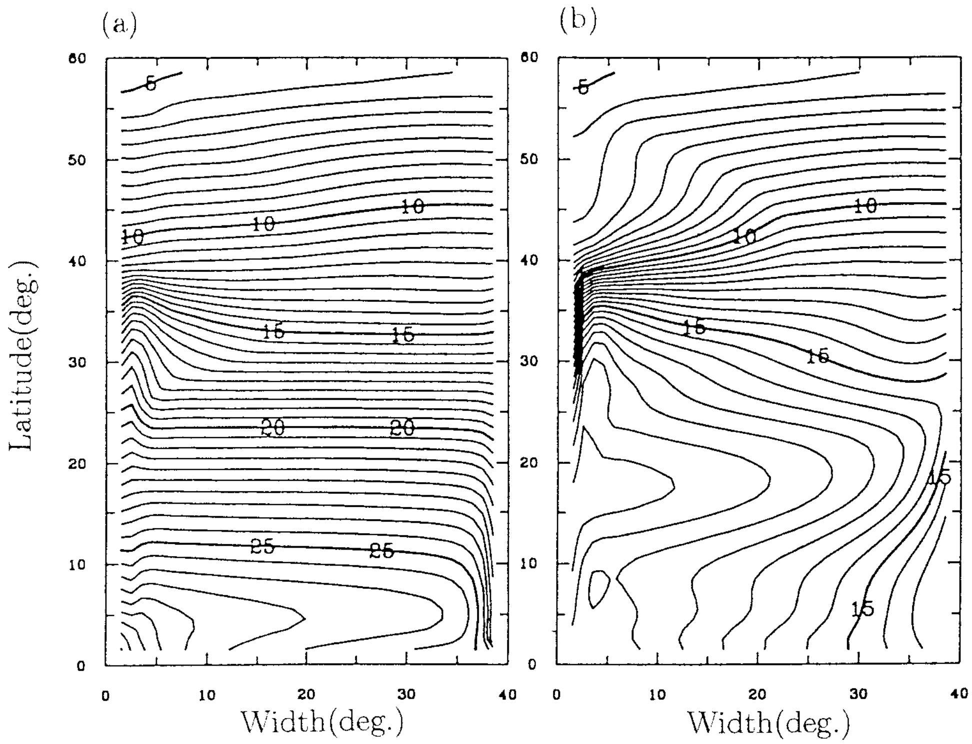

FIG. 4. Horizontal distributions of potential temperature after 40 years at (a) the first level ($z = -2$ m) and (b) the 7th level ($z = -77.6$ m) for RUN-1. The contour interval is 0.5°C.

process in the model ocean is estimated to be about 15 years, consistent with the estimate based on the trajectory analysis. This result also agrees with the ventilation age of 10 to 16 years calculated by CB.

4. Effects of the nonzonal zero wind stress curl line

In this section, we will compare the results for the nonzonal ZWCL (RUN-2 and RUN-3) and the results for the zonal ZWCL (RUN-1). Since it is difficult to describe differences between these experiments by comparing velocity and temperature fields, we use a trajectory analysis and a tracer-injection experiment instead.

Figure 7 is a schematic diagram illustrating the different situations for the zonal and nonzonal ZWCL cases. In RUN-1, the ZWCL coincides with the boundary between the subarctic and subtropical gyres, which is defined by the Sverdrup streamfunction, ψ, equal to zero. Therefore, downwelling occurs everywhere in the subtropical region and upwelling occurs everywhere in the subarctic region (Fig. 7a). In RUN-2 and RUN-3, however, the ZWCL does not coincide with the gyre boundary. This results in two characteristic regions (Fig. 7b): There is an upwelling region in the northwestern corner of the subtropical gyre and a downwelling region that extends northward in the northeastern corner of the subtropical gyre. The existence of these two regions in RUN-2 and RUN-3 causes several significant differences to RUN-1.

Figure 8 shows tracer concentrations of all three runs on meridional sections at 10°, 20°, and 30°. A comparison between RUN-1 and RUN-2 reveals that the local maximum of tracer concentrations in the ventilated layer is located deeper in the case with nonzonal ZWCL. Moreover, the local maximum has a larger tracer concentrations in RUN-2. These two tendencies are more apparent in RUN-3, where the tilt of the ZWCL is exaggerated. These experiments do not necessarily suggest a linear increase in these results with increased tilt of the ZWCL, but they do show that the results become significantly more exaggerated with the larger tilt. In RUN-2 and RUN-3, where the downwelling region extends northward, the subarctic surface water starts to subduct in higher (therefore colder) latitudes, where tracer concentrations are high. The subducted water penetrates deeper since it downwells from higher latitudes (see, e.g., Fig. 8c). Compared to RUN-1, tracer concentrations have higher values at the same depth and their local maximum exists deeper in the water column on the meridional section at 30° in RUN-2 and RUN-3. Consequently, tracer moves from the subarctic surface to the western boundary region by deeper path in the nonzonal runs (Figs. 8a and 8b). Thus, the ventilated region becomes deeper in RUN-2 and RUN-3.

Figure 9 shows trajectories of water particles released

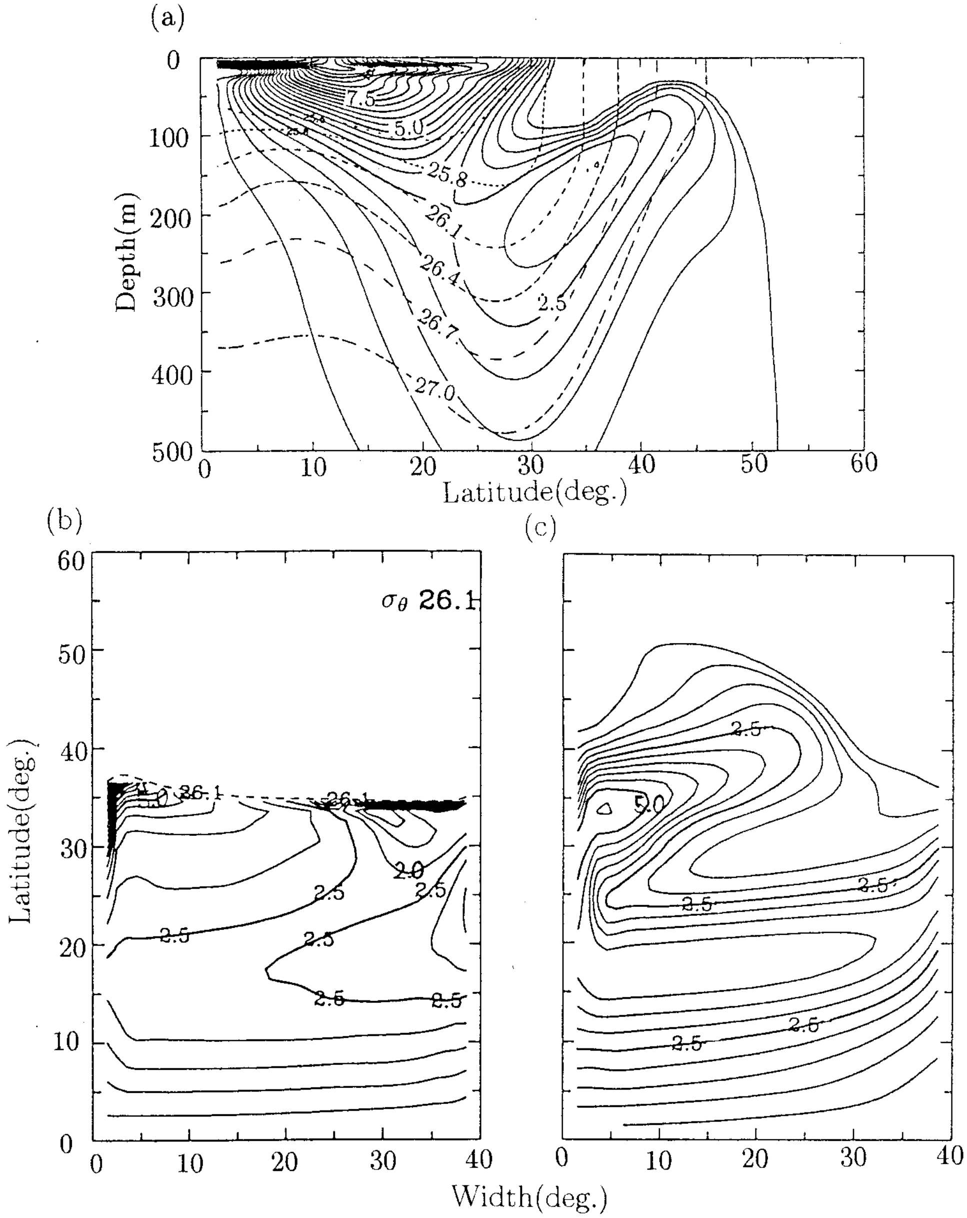

FIG. 5. (a) Meridional sections of the potential vorticity (solid curves) and potential density (dashed curves) in the middle of basin after 40 years. Contours are drawn for potential density from 25.5 to 27.0 with an interval of 0.3 sigma unit. (b) Potential vorticity on the isopycnal surface $\sigma_\theta = 26.1$. (c) Potential vorticity on the 8th level ($z = -108.5$ m). The contour interval for potential vorticity is 0.5×10^{-9} cm^{-1} s^{-1} in all three panels.

in the western boundary region in the 5th level ($z = -35.6$ m) in (a) RUN-1 and (b) RUN-2. The trajectories are followed for 15 years. After being released in the western boundary region, most of the water particles circulate as follows. First, they upwell into the subarctic surface and are advected southeastward by the Ekman flow. Second, they subduct into the subtropical gyre following the Sverdrup regime and are carried back to the western boundary region. Finally, some particles are advected into the equatorial region, while others are advected back to the subtropical gyre. The pathways of water particles lie farther to the west in the region between 20° and 35°N in RUN-2 than in RUN-1. In RUN-2, where the subtropical upwelling region exists, water particles in the western boundary region move upward with larger velocities due to the upwelling and reach the surface faster than particles in RUN-1. Therefore, the position of the outcrop area shifts westward, resulting in a smaller pool region (Fig. 9b) and the trajectories of the water particles shift westward. This al-

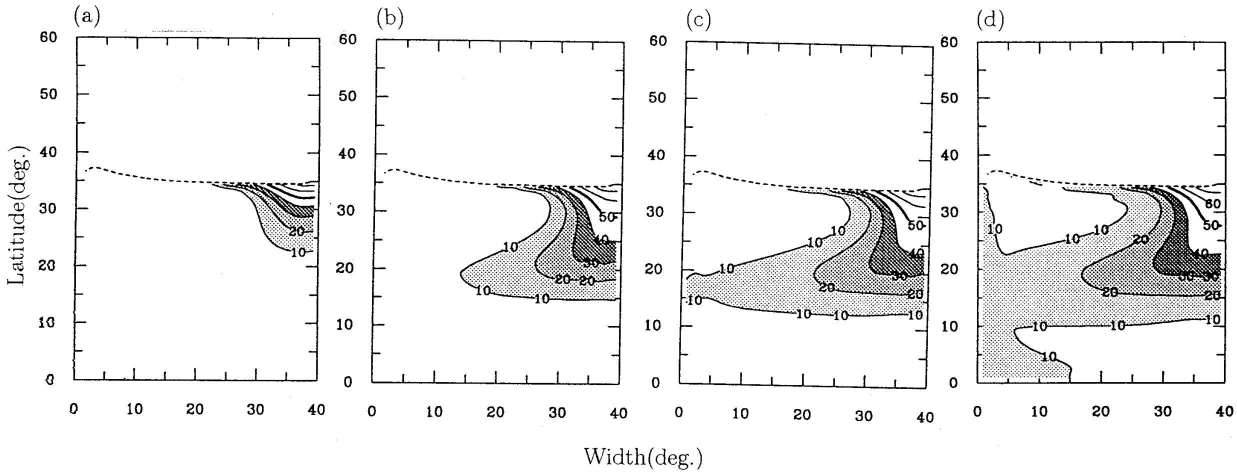

FIG. 6. Temporal evolution of tracer distribution on the isopycnal surface $\sigma_\theta = 26.1$ (a) 3, (b) 5, (c) 7, and (d) 15 years after the tracer was introduced. The contour interval is 10 and regions with concentrations from 10 to 40 are shaded.

lows more water particles to return to the subtropical circulation in RUN-2 than in RUN-1. Water particles that reach the equatorial region upwell there and move back toward the subtropical gyre due to the Ekman flow.

Figure 10 shows the first five years of the time series of σ_θ of the trajectories shown in Fig. 9. We will discuss the σ_θ of water particles penetrating just into the thermocline, the first stage of subduction. For clarity only the first five years are shown. Originally, water particles have various values of σ_θ in the western boundary region. When these particles are advected into the subarctic surface region, the values of σ_θ are renewed by the surface heat flux. Once they are subducted into the ventilated region, the values of σ_θ become fairly constant. In RUN-1, subducted particles have σ_θ values ranging from 25.9 to 26.1. In contrast, particles have σ_θ values ranging from 25.8 to 26.2 in RUN-2. This indicates that the tilting of the ZWCL can cause the subducted water particles to have a wider range of σ_θ. This result can be explained as follows. The subtropical upwelling region causes water particles to upwell faster and to surface in warmer latitudes, which allows them to have lower σ_θ in the western part of the basin. In addition, the northward extension of the downwelling region causes the particles to subduct in colder latitudes, which allows higher σ_θ in the east. These two effects

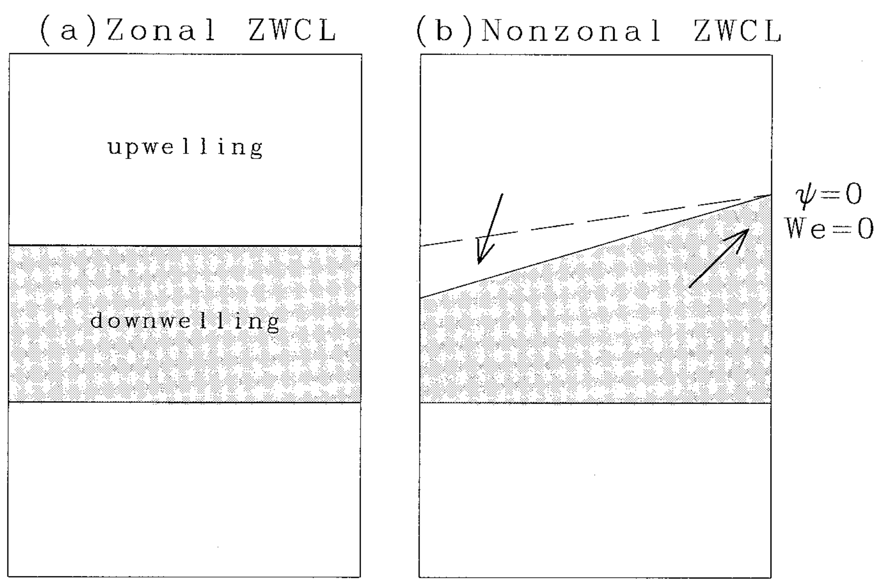

FIG. 7. A schematic diagram illustrating (a) the zonal ZWCL and (b) nonzonal ZWCL cases. In each panel, the dashed line denotes the boundary between the subarctic and subtropical gyres, and the bold line indicates the We (Ekman pumping velocity) = 0. The downwelling region is shaded. The two lines are overlapped in (a). In (b), the two characteristic features are indicated by arrows.

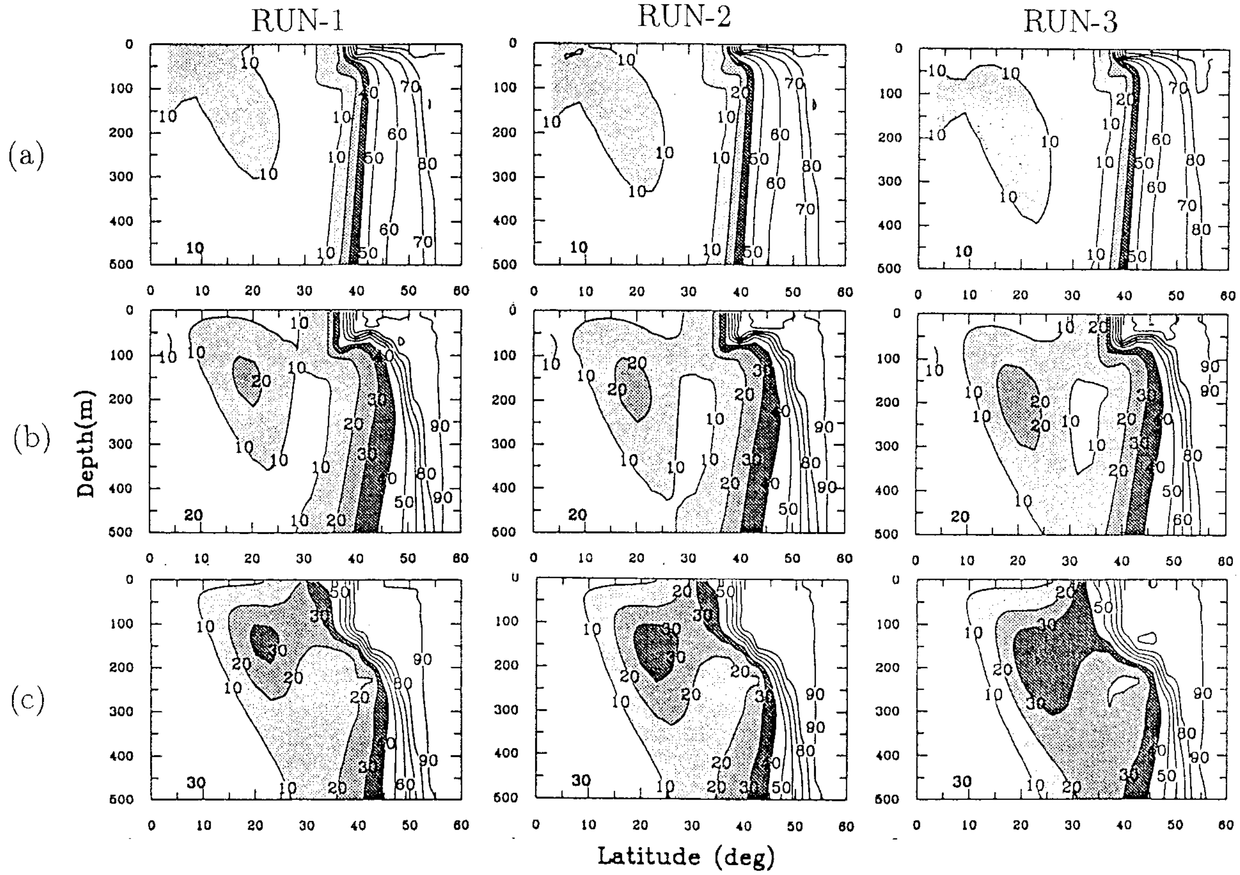

FIG. 8. Meridional sections of tracer concentrations at (a) 10°, (b) 20°, and 30° in RUN-1 (left), RUN-2 (middle), and RUN-3 (right) 15 years after the tracer was introduced.

result in the wider range of σ_θ. A closer examination of Figs. 9 and 10 reveals that water particles of lower (higher) σ_θ subduct in the relatively western (eastern) part of the subtropical gyre. If subducted water has a wider range of σ_θ, tracers will be distributed on more isopycnal surfaces. This suggests that tracers can be found on a wide range of isopycnal surfaces in the real ocean, where the actual ZWCL is nonzonal.

The results shown in Figs. 8–10 indicate that solutions are quite different in RUN-1 and RUN-2 despite the fact that the tilt of the ZWCL is not large in the latter case. This suggests that the subduction process is very sensitive to the positional relation between the ZWCL and the line defined by $\psi = 0$.

5. Summary and discussion

We have studied the subduction process using a general circulation model (Fig. 2). Three different wind stress fields (Fig. 3) are applied to a model ocean and the different responses are compared. One of the wind fields has a zonal ZWCL, the other two have a nonzonal ZWCL, more realistic of the climatological mean field (Fig. 1a). In these latter two experiments, the line defined by $\psi = 0$ and the zero wind stress curl line (Fig. 1) lie at angles to each other.

The results for the zonal ZWCL experiment are discussed in section 3. A reasonable potential temperature field and western boundary current is produced in this highly idealized numerical model (Fig. 4). Low q water, due to the negative heat flux in the western boundary outflow region, advects into the boundary between the subarctic and subtropical gyres. This water then flows southwestward into the subtropical gyre, penetrating deep into the water column. Finally, it reaches the boundary between the subtropical and tropical gyres (Fig. 5). The distribution of the subarctic tracer reveals the presence of the three characteristic regions as described in LPS; a pool region, a ventilated region, and a shadow zone. The timescale of the subduction process is estimated to be about 15 years in this model ocean (Fig. 6).

In this study, our main purpose is to gain a general understanding of the subduction process and not to simulate a detailed structure of general circulation in any specific ocean. For computational efficiency, the model basin width is only 40°, narrower than both the Atlantic and Pacific. It is possible that the timescale of the sub-

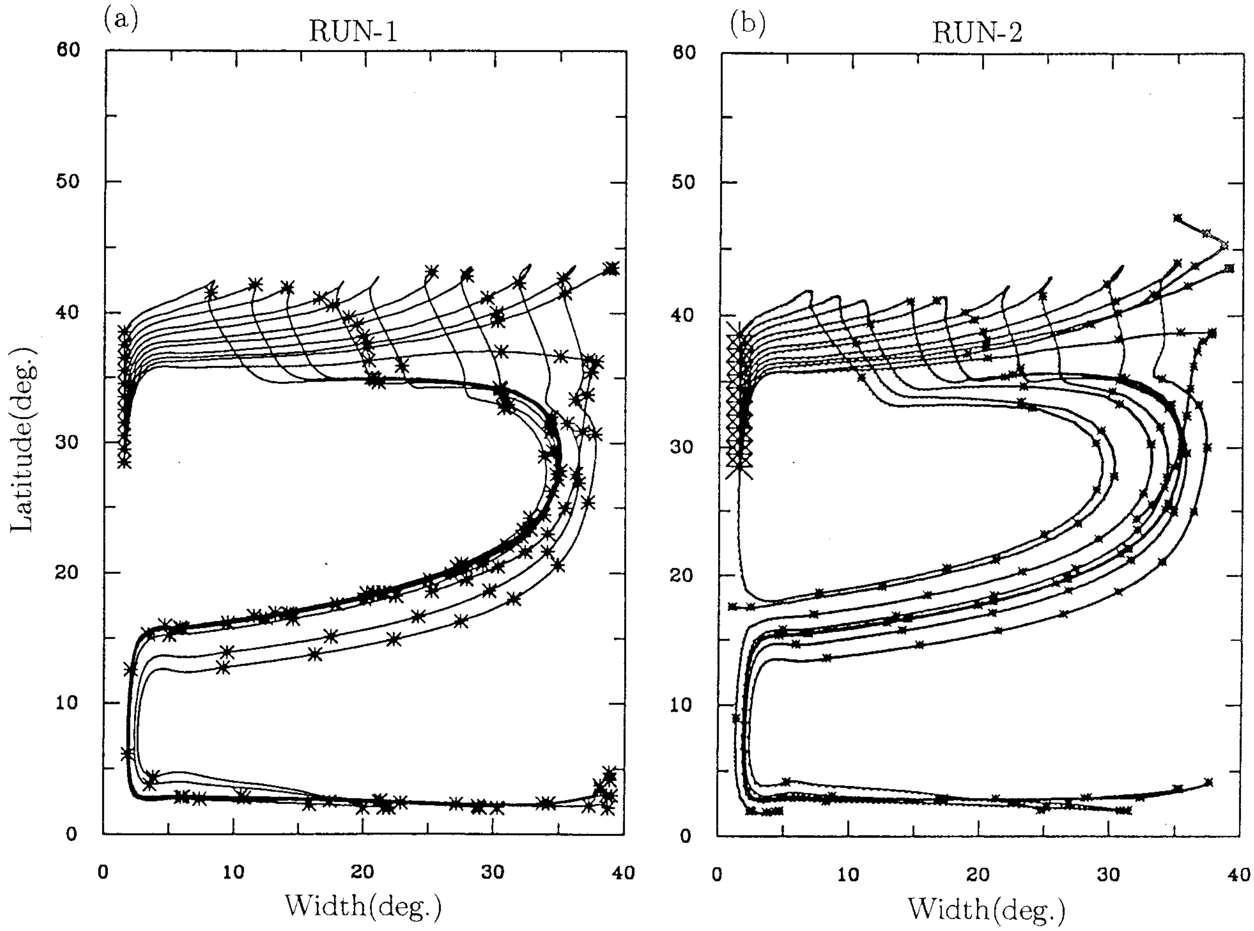

FIG. 9. Trajectories of water particles for 15 years since their release in the region of the western boundary current at $z = -35.6$ m in (a) RUN-1 and (b) RUN-2. Asterisks on each trajectory denote locations of particles at the beginning of each year.

duction process is longer in a wider basin. In order to examine this problem, we conducted the same tracer-injection experiment as described in the appendix using a model whose basin width was 74°. Although this model was designed for other purposes, and the wind stress and the atmospheric temperature are not identical to the model used in the present study, it was still useful to obtain some insight on the effect of the basin width. In this additional study, tracer circulated through the subtropical gyre in 20 years, but took only about 15 years to reach the equatorial gyre. This similar timescale in this new experiment and that of the narrower basin experiment is probably caused by the use of the same Sverdrup velocity in both experiments and suggests that basin width does not significantly affect the subduction timescale.

Results for the zonal and nonzonal ZWCL cases are compared in section 4. When the ZWCL is not zonal, two characteristic regions exist (Fig. 7). These two regions become larger as the tilt of the ZWCL increases and are considered to be important for understanding the source area for a water mass. For example, the presence of the subtropical upwelling region is thought to be important in the formation of the MSM (Yuan and Talley 1992) since the source region corresponds to the region of the upwelling. The distribution of the subarctic tracer shows that the local maximum concentration in the ventilated layer has higher values and exists deeper in the water column for the nonzonal ZWCL. This implies that the ventilated region becomes deeper (Fig. 8) with increased tilt of the ZWCL. The trajectory analysis shows that the nonzonal ZWCL results in a smaller pool region (Fig. 9) and subducted water particles having a wider range of σ_θ (Fig. 10).

Without salinity effects in these experiments, it is difficult to distinguish MSM from SSM; we can only analyze the tendency of the subarctic tracer distribution. In the real ocean, MSM is distributed mainly on the $\sigma_\theta = 26.2$ surface, which is deeper than the SSM layer, and lies to the west of SSM. In addition, the SSM region is thought to surface in the northwestern corner of the subtropical gyre, which might be affected by the existence of the subtropical upwelling region. In our experiments, we speculate that MSM may occur when the

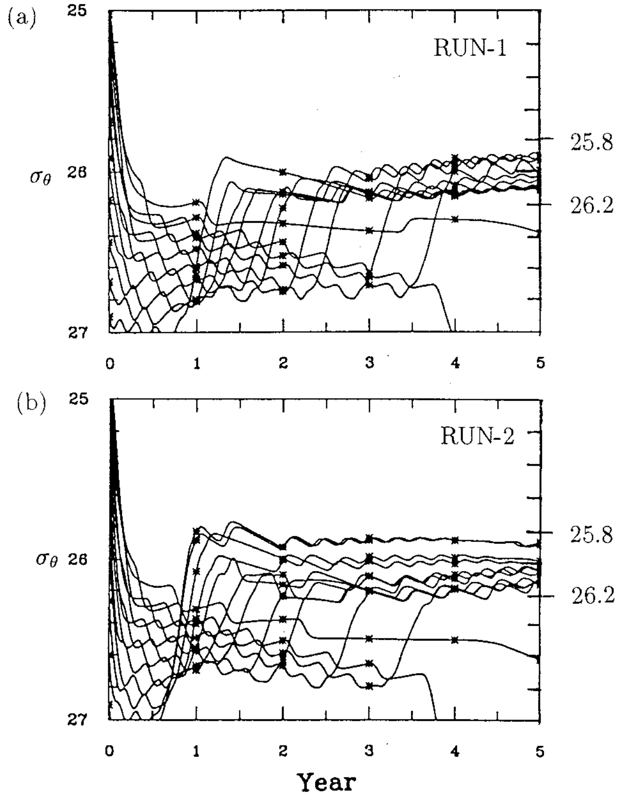

FIG. 10. Temporal changes of σ_θ along the trajectories of the water particles shown in Fig. 9 in (a) RUN-1 and (b) RUN-2. Only the first 5 years are shown.

tilt of the ZWCL causes the tracer distribution to shift westward and deeper. Our results suggest that MSM is more likely to form in the nonzonal case than in the zonal case.

For the nonzonal ZWCL, the subarctic surface tracer starts to subduct along the outcrop line of colder σ_θ values since the northward extension of the downwelling region—the reason that the ventilated region becomes deeper. In the real ocean, the distribution of the subarctic tracer is affected by surface conditions in both the subtropical and subarctic gyres. However, the deeper the water particles subduct, the less the surface conditions can alter their properties. Therefore, the existence of the realistic, nonzonal ZWCL suggests that the subarctic tracer can reach the western boundary region or the equatorial region with properties relatively unchanged. The shrinkage of the pool region, caused by the nonzonal ZWCL, is also seen by Talley (1985) and Rhines and Schopp (1991). As the inclination of the ZWCL becomes larger, the subducted water in the ventilated region has a wider range of σ_θ. This suggests that subarctic tracers can be found on a wide range of isopycnal surfaces in the real ocean.

In conclusion, we have identified three characteristic effects of the nonzonal ZWCL on the subduction process: 1) shrinkage of the pool region, 2) deeper ventilated region, and 3) wider range of water properties. These effects are apparent for both the exaggerated tilt of the ZWCL and the realistic tilt. In this study, we have only considered a steady wind stress fields, it is likely that both seasonal and decadal variations of winds have significant effects on the subduction process. Furthermore, we need to include a salinity equation in order to understand the source of water masses in the real ocean. We are currently planning to investigate these and other related issues.

Acknowledgments. Most of the numerical calculations were carried out on a NEC SX-3/44R computer at the Computing Center of Tohoku University. During the course of this study, we had useful discussions with members of the Physical Oceanography Group at Tohoku University and Hokkaido University. We would also thank Drs. Kensuke Takeuchi and Yasushi Fukamachi, and Ms. Stephanie Dutkiewicz at the University of Rhode Island for their assistance in completing the manuscript. Comments from Dr. Julian P. McCreary were also appreciated. Two reviewers helped us improve our paper. We express our thanks to them.

APPENDIX

The Equation for Tracer Concentrations

In the tracer-injection experiment, an additional equation for tracer concentrations Tr is used:

$$\mathrm{Tr}_t + \Gamma(\mathrm{Tr}) = F^{\mathrm{Tr}} + \text{sources},$$

where

$$F^{\mathrm{Tr}} = \left(\frac{A_{\mathrm{TV}}}{\delta}\mathrm{Tr}_z\right)_z + \frac{A_{\mathrm{TH}}}{a^2}\nabla^2\mathrm{Tr}.$$

Here Tr ranges from 0 to 100. The ''source'' term can be nonzero only at the surface of the subarctic region, which is located north of the line defined by $\psi = 0$. It is given by

$$\text{source} = \begin{cases} \kappa(100 - \mathrm{Tr}_{z=0}), & \text{if } z = 0 \\ 0, & \text{if } z \neq 0, \end{cases}$$

where κ is a constant, 0.5 day^{-1}. The source term is identically zero in other regions.

REFERENCES

Bryan, K., 1969: A numerical method for the study of the circulation of the World Ocean. *J. Comput. Phys.,* **4,** 347–376.

Cox, M. D., and K. Bryan, 1984: A numerical model of the ventilated thermocline. *J. Phys. Oceanogr.,* **14,** 674–687.

Haney, R. L., 1971: Surface thermal boundary condition for ocean circulation models. *J. Phys. Oceanogr.,* **1,** 241–248.

Harrison, D. E., 1988: On climatological monthly mean wind stress and wind stress curl fields over the World Ocean. *J. Climate,* **1,** 57–70.

Huang, R. X., 1988: On the boundary value problems of the ideal-fluid thermocline. *J. Phys. Oceanogr.,* **18,** 619–641.

——, 1989: On the three-dimensional structure of the wind-driven circulation in the North Atlantic. *Dyn. Atmos. Oceans,* **15,** 117–159.

Levitus, S., 1982: *Climatological Atlas of the World Ocean.* NOAA Prof. Paper No. 13, U.S. Govt. Printing Office, 173 pp.

Luyten, J., J. Pedlosky, and H. Stommel, 1983: The ventilated thermocline. *J. Phys. Oceanogr.,* **13,** 292–309.

Munk, W. H., 1950: On the wind-driven ocean circulation. *J. Meteor.,* **7,** 79–93.

Pedlosky, J., 1986: The buoyancy and wind-driven ventilated thermocline. *J. Phys. Oceanogr.,* **16,** 1077–1087.

——, and P. Robbin, 1991: The role of the finite mixed-layer thickness in the structure of the ventilated thermocline. *J. Phys. Oceanogr.,* **21,** 1018–1031.

——, W. Smith, and J. R. Luyten, 1984: On the dynamics of the coupled mixed layer-thermocline system and the determination of the oceanic surface density. *J. Phys. Oceanogr.,* **14,** 1159–1171.

Reid, J. L., 1973: The shallow salinity minima of the Pacific Ocean. *Deep-Sea Res.,* **20**(Suppl.), 51–68.

Rhines, P. B., and R. Schopp, 1991: The wind-driven circulation: Quasi-geostrophic simulations and theory for nonsymmetric winds. *J. Phys. Oceanogr.,* **21,** 1438–1469.

Stommel, H., 1948: The westward intensification of wind-driven ocean current. *Trans. Amer. Geophys. Union,* **29,** 403–406.

Talley, L. D., 1985: Ventilation of the subtropical North Pacific: The shallow salinity minimum. *J. Phys. Oceanogr.,* **15,** 633–649.

Tsuchiya, M., 1982: On the Pacific upper-water circulation. *J. Mar. Res.,* **40**(Suppl.), 777–799.

UNESCO, 1981: Tenth report of the joint panel on oceanographic tables and standards. UNESCO Tech. Papers in Marine Science 36 pp.

Welander, P., 1971: Some exact solutions to the equation describing an ideal-fluid thermocline. *J. Mar. Res.,* **29,** 60–68.

Williams, R. G., 1991: The role of the mixed layer in setting the potential vorticity of the main thermocline. *J. Phys. Oceanogr.,* **21,** 1803–1814.

Yuan, X., and L. D. Talley, 1992: Shallow salinity minima in the North Pacific. *J. Phys. Oceanogr.,* **22,** 1302–1316.